공학석사 학위논문

Understanding Lithium-Ether Co-Intercalation in Graphite for Rechargeable Lithium-Ion Battery Electrode

흑연에서의 용매-리튬 이온 삽입 반응을 이용한 리튬 이온 이차전지 소재 개발

2017 년 08 월

서울대학교 대학원

재료공학부

임 경 미

Understanding Lithium–Ether Co–Intercalation in Graphite for Rechargeable Lithium–Ion Battery Electrode

A THESIS SUBMITTED TO
DEPARTMENT OF MATERIALS SCIENCE AND ENGINEERING
SEOUL NATIONAL UNIVERSITY

FOR THE DEGREE OF MASTER

August 2017

By

Kyungmi Lim

Supervisor

Kisuk Kang

Abstract

Understanding Lithium-Ether Co-intercalation in Graphite for Rechargeable Lithium-Ion Battery Electrode

Kyungmi Lim

Department of Materials Science and Engineering

College of Engineering

Seoul National University

The intercalation of lithium ions into graphite electrode is the key underlying mechanism of modern lithium-ion rechargeable batteries. However, co-intercalation of lithium-ions and solvent into graphite is considered undesirable because it can trigger the exfoliation of graphene layers and destroy the graphite crystal, resulting in poor cycle life. Here, we demonstrate that the $[\text{lithium–solvent}]^+$ intercalation does not necessarily cause exfoliation of the graphite electrode and can be remarkably reversible

with appropriate solvent selection. First-principles calculations suggest that the chemical compatibility of the graphite host and [lithium–solvent]$^+$ complex ion strongly affects the reversibility of the co-intercalation, and comparative experiments confirm this phenomenon. Moreover, it is revealed that [lithium–ether]$^+$ co-intercalation of natural graphite electrode enables much higher power capability than normal lithium intercalation, without the risk of lithium metal plating. To be specific, [lithium-ether]$^+$ co-intercalation shows capacity retention of approximately 87% of the theoretical capacity at current density of 1 A g^{-1}. This unusual high rate capability of the co-intercalation is attributable to the (i) absence of the last desolvation step, (ii) negligible formation of the solid-electrolyte interphase on graphite surface, and (iii) partially capacitive charge-transfer mechanism. This work constitutes the first step toward the utilization of fast and reversible [lithium–solvent]$^+$ complex ion intercalation chemistry in graphite for rechargeable battery technology.

Keywords: Graphite, lithium-ion batteries, co-intercalation, high-power batteries, first-principles calculations

Student Number: 2015-20879

The content of this thesis has been published in *Advanced Energy Materials*, reprinted with permission from H. Kim *et al*. Exploiting Lithium-Ether Co-Intercalation in Graphite for High-Power Lithium-Ion Batteries, *Adv. Energy Mater*. **2017**, 1700418 (DOI: 10.1002/aenm.201700418)

Contents

List of Figures

List of Tables

1. Introduction

Graphite can serve as an intercalation host for versatile guest species in its galleries, forming binary/ternary graphite intercalation compounds.[1] Its capability of accommodating lithium ions via intercalation combined with its low cost and abundance has made graphite a standard anode for modern lithium-ion batteries (LIBs).[2-6] In the early development of LIBs employing graphite anodes, the search for an appropriate electrolyte system was important with respect to not only the ionic conductivity and/or electrochemical window but also its compatibility with the graphite anode.[7-13] The use of propylene carbonate (PC)-based electrolytes resulted in rapid capacity degradation of graphite anodes during battery operation despite their high electrochemical stability.[14, 15] Researchers observed that the degradation was related to the co-intercalation of lithium ions and the large solvent molecules, which led to exfoliation of the graphene layers.[14, 16-18] Thus, subsequent efforts have been made to prevent co-intercalation in graphite anodes for LIBs, which naturally led to the perception that ion–solvent co-intercalation is detrimental in this system.[16, 17, 19] However, recently, Jache *et al.* and our group independently reported the potential of graphite as an anode material for sodium-ion batteries (NIBs) by employing the co-intercalation of sodium ions and solvent molecules.[20, 21] In this

system, graphite accommodated the intercalation of [sodium–ether]$^+$ complex ions without noticeable side reactions such as the exfoliation of graphite. Moreover, the graphite anode provided superior cycle stability (more than 2,500 repetitive electrochemical cycles), demonstrating the reversibility of the co-intercalation chemistry despite the large volume expansion of ~345%.[20-23] Subsequent research conducted by Cui *et al.* also demonstrated the practical feasibility of [sodium–ether]$^+$ complex ion intercalation in NIBs and sodium-ion capacitors with good cycle stability.[24, 25]

Our current study started from a simple question of the contradiction between reversible [sodium–solvent]$^+$ co-intercalation and well-known instability of [lithium–solvent]$^+$ co-intercalation in graphite electrodes.[16, 20-22, 26] Although lithium and sodium share similar chemical and electrochemical properties to some extent, they exhibit surprisingly distinct behaviors in the co-intercalation. Moreover, the origin of the severe exfoliation of graphite associated with the lithium ion–solvent complex despite the smaller size of lithium ions compared with sodium ions is unclear. This work unveils the importance of the chemical compatibility of the co-intercalated solvent in determining whether exfoliation occurs in the lithium co-intercalation. In addition, it is demonstrated that the [lithium–ether]$^+$ complex ion de/intercalation in graphite is remarkably reversible, enabling a

cycle life of more than 200 cycles, and that the previously reported instability of ether-based lithium co-intercalation is not due to the intrinsic irreversibility in graphite.[26] Furthermore, the graphite electrode based on the co-intercalation is shown to be capable of delivering a high power capability, retaining approximately 87% of its theoretical capacity at a current density of 1 A g^{-1} without the risk of lithium metal plating. The observed high power capability of the co-intercalation is counterintuitive, considering that the intercalation of large guest ions in the host has been believed to be sluggish. The origin of this unusual phenomenon is discussed in relation to the desolvation kinetics, nature of the solid electrolyte interphase (SEI) layer, and charge storage mechanism.

2. Experimental Section

2.1. Materials

Natural graphite (average size: ~100 μm) was purchased from Bay Carbon Inc. and used without any modification. Electrolytes were carefully prepared to maintain low H2O content (<20 ppm). Lithium salts (LiTF and LiTFSI) and molecular sieves were stored in a vacuum oven at 180°C. Dried lithium salts were dissolved in a diethylene glycol dimethyl ether (DEGDME) solvent at 1 M. The solution was stirred at 80°C for 3 days. Molecular sieves were added in the solution to remove residual H2O from the electrolyte solution.

2.2. Electrode preparation and electrochemical measurements

Graphite electrodes were prepared by mixing the active material (natural graphite, 90 wt%) with polyvinylidene fluoride binder (PVDF, 10 wt%) in an N-methyl-2-pyrrolidone (NMP) solvent. The resulting slurry was uniformly pasted onto Cu foil, dried at 120°C for 1 hour and roll-pressed. The average electrode thickness and loading density were ~50 μm and ~5 mg cm-2. Test cells were assembled in a glove box into a two-electrode configuration with a lithium metal counter electrode. Full cells were constructed with excessive amount of $LiFePO_4$ as a cathode material. A separator of grade

GF/F (Whatman, USA) was sonicated in acetone and dried at 120°C before use. Electrochemical profiles were obtained over a voltage range of 2.5 to 0.01 V using a multichannel potentio-galvanostat (WonATech).

2.3. Characterization

The structure of the samples was analyzed using an X-ray diffractometer (XRD, D2PHASER, Bruker, USA) using Cu Kα radiation. The morphology of the samples was verified using field-emission scanning electron microscopy (FE-SEM, SUPRA 55VP, Carl Zeiss, Germany). The electrode after cycling was analyzed using X-ray photoelectron spectroscopy (XPS, PHI 5000 VeraProbe™) and Raman spectroscopy (high resolution dispersive Raman microscope, Horiba Jobin Yvon, France). Gas evolution during battery operation was characterized using differential electrochemical mass spectrometry (HPR-20, Hiden Analytical). SEI was observed using high-resolution transmission electron spectroscopy (HR-TEM, JEM2100F, JEOL, Japan). Ionic conductivity of electrolytes was measured with portable conductivity meter (Oakton waterproof portable CON 610 conductivity meter, Singapore).

2.4. Calculation details

First-principles calculations were conducted to obtain the HOMO/LUMO levels and the energy of [Li-solvent$_x$]$^+$ complexes (solvents: PC, EC, DMC, and DEGDME) and isolated solvent molecules using the Gaussian 09 code.[57] All geometries were optimized with the B3LYP/6-311G (3df) level of exchange-correlation functionals and basis sets.[58, 59] Based on the calculated energies of molecules, desolvation energy was obtained using the following definition:

$$E_{des,x} = E_{[Li-solvent_{x-1}]^+} + E_{solvent} - E_{[Li-solvent_x]^+}.$$

Here, $E_{[Li-solvent_{x-1}]^+}$, $E_{[Li-solvent_x]^+}$ and $E_{solvent}$ represents the energy of [Li-solvent$_{x-1}$]$^+$, [Li-solvent$_x$]$^+$ and isolated solvent molecule, respectively.

3. Results and Discussion

3.1. Capacity degradation of co-intercalation and structural integrity of graphite

The electrochemical behavior of lithium co-intercalation in graphite was examined using an ether-based electrolyte as shown in Figure 1a, which presents the discharge/charge profile using 1 M lithium trifluoromethanesulfonate (LiTF) in diethylene glycol dimethyl ether (DEGDME).[23, 26] The overall profile in the first cycle clearly differs from the characteristic lithium ion intercalation in conventional LIBs but agrees with the previous report of lithium ion/solvent molecule co-intercalation and is similar to that of the typical [sodium–ether]$^+$ complex ion intercalation shown in Figure 1b.[20, 26] However, the specific capacity decreases rapidly during repeated battery cycling; only a fraction of the initial capacity (~20 mAh g^{-1}) was maintained after 20 cycles, which is consistent with previous speculations.[16, 26] Changing the salt in the electrolyte from LiTF to lithium trifluoromethanesulfonimide (LiTFSI) for improved chemical stability[27, 28] did not improve the cycle stability, as observed in Figure 1c. In contrast, changing the salt from LiTF to NaTF, *i.e.*, [sodium–ether]$^+$ complex ion intercalation, dramatically improved the cycle performance by more than 200 times using the same cell configuration (Figure 1d).[20-22]

To understand this distinct behavior of the graphite electrode, we first characterized the structural change upon repeated lithium co-intercalation in the ether-based electrolyte using *ex-situ* X-ray diffraction (XRD), as shown in Figure 2. The XRD patterns for the first cycle indicate that the graphite electrode undergoes successive phase transformations, which is consistent with our previous work.[26] The evolution of the XRD patterns is analogous to that of [sodium–ether]$^{+}$ complex ion intercalation into graphite, indicating a typical co-intercalation staging phenomenon.[26, 29] The expansion along the *c*-axis is slightly smaller for lithium than for sodium during the co-intercalation (approximately 334% and 349%, respectively, in Figure 3a and b).[26] Interestingly, Figure 1d shows that the graphite crystal structure did not undergo any noticeable degradation with the repeated cycles. The XRD patterns of the graphite electrode were nearly unchanged, and the pristine layered structure was maintained after 2, 3, and 10 cycles of the co-intercalation. This finding contradicts the observation that significant cycle degradation occurs after 10 cycles, as shown in Figure 1a, c and d, suggesting that the structural degradation of the graphite crystal may not be the main cause of the instability of the lithium cells. We further confirmed that no noticeable morphological change (*i.e.*, exfoliation) occurred in the cycled graphite electrode in the ether-based lithium cell, as shown in Figure 4a, which indicates that the morphology of the pristine graphite was well

preserved after cycling. No significant increase of the structural defects in the graphite was detected by Raman spectroscopy analysis after the repeated lithium ion co-intercalation (Figure 4b).

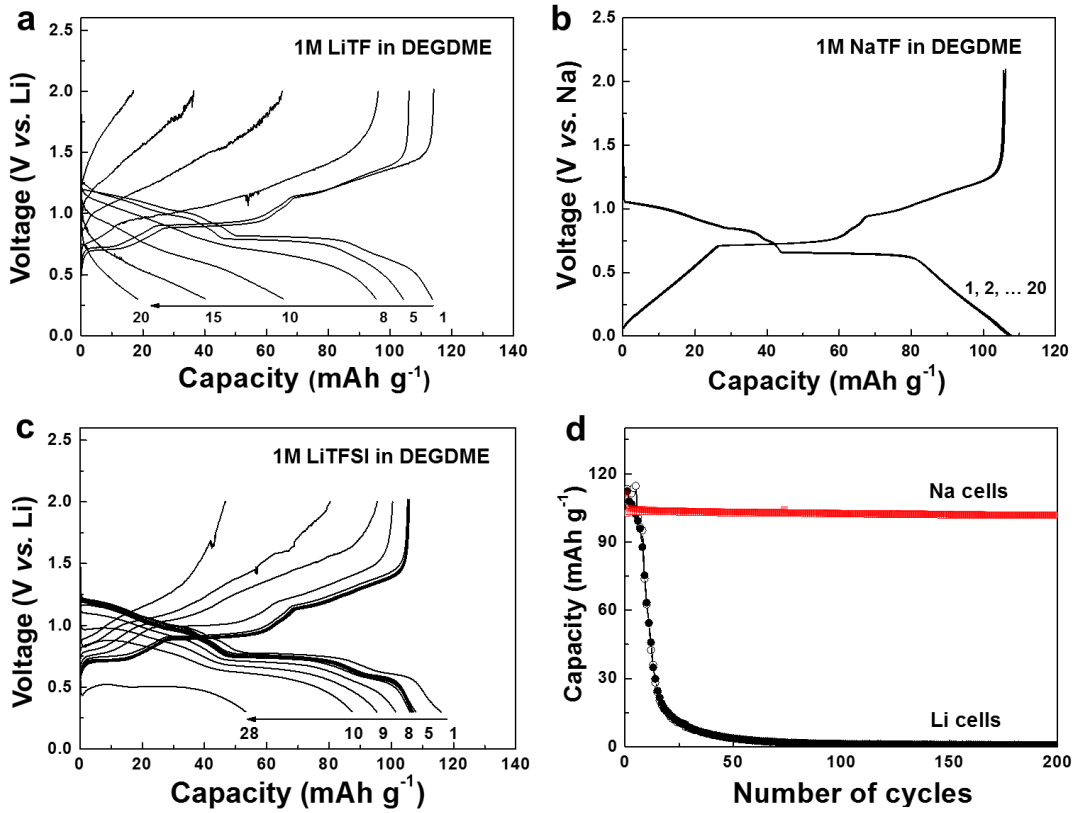

Figure 1. (a) Charge/discharge profiles of graphite/lithium cells using 1 M LiTF in DEGDME electrolyte. (b) Typical charge/discharge profiles of [sodium–ether]$^{+}$ complex co-intercalation using 1 M NaTF in DEGDME. (c) Charge/discharge profiles of graphite/lithium cells using 1M LiTFSI in DEGDME electrolyte. (d) Cycle performance of graphite anode in sodium and lithium cells using DEGDME electrolytes (black: 1 M LiTF in DEGDME; red: 1 M NaTF in DEGDME).

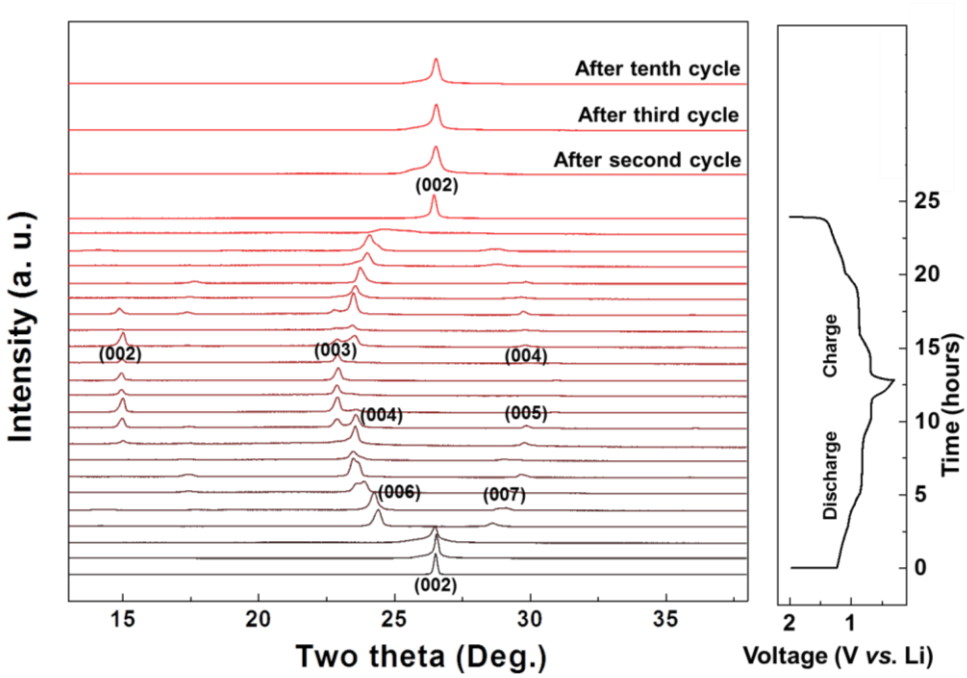

Figure 2. *Ex-situ* XRD analysis of the structural evolution of [lithium-ether]$^{+}$ complex co-intercalation during intercalation and deintercalation into/out of graphite. XRD patterns of graphite after second, third, and tenth cycles are also shown.

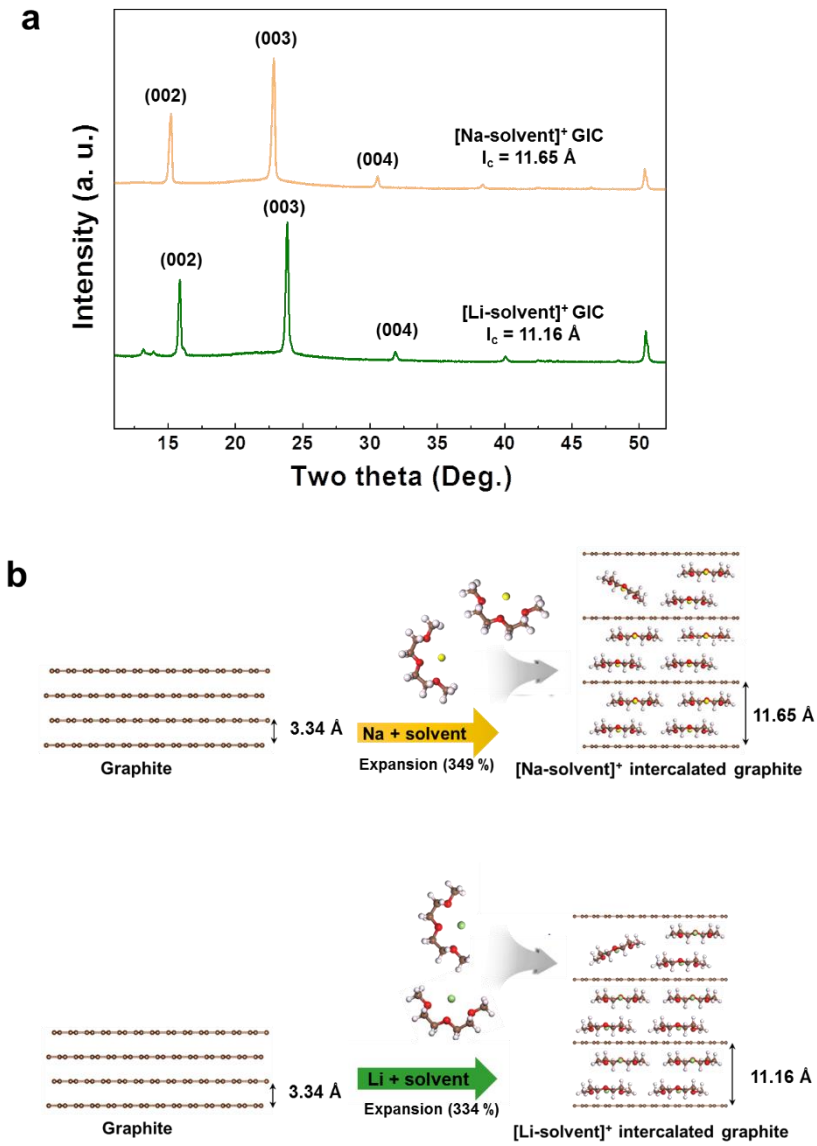

Figure 3. (a) XRD patterns of the sodiated (above) and lithiated (below) graphite electrodes. Schematics of (b) sodiated (above) and lithiated (below) graphite electrodes.

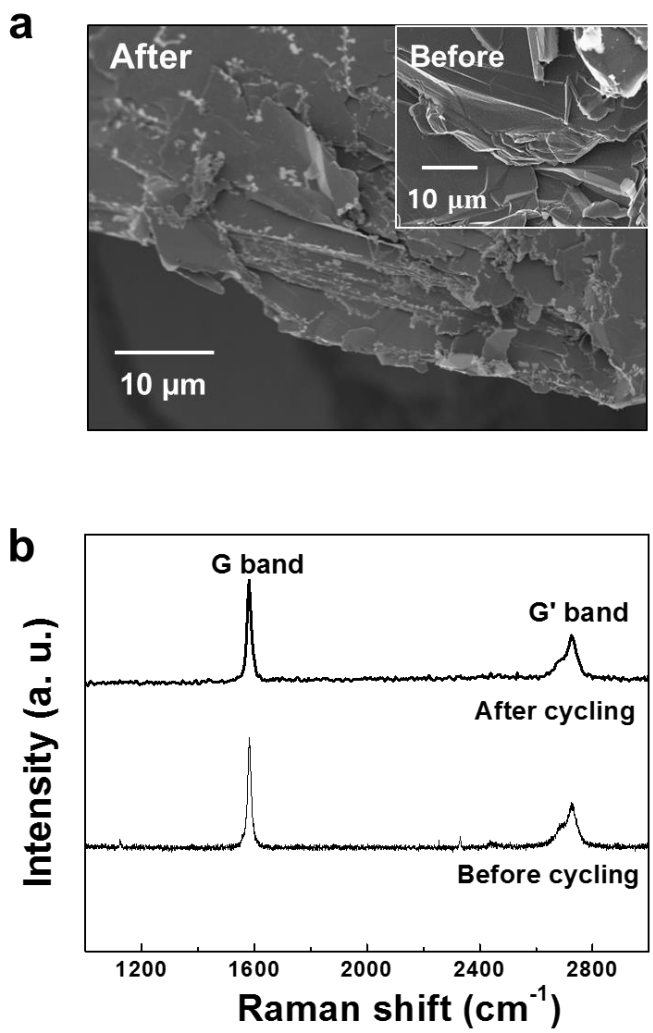

Figure 4. (a) SEM image of graphite electrode after cycling with 1 M LiTFSI in DEGDME (inset: pristine graphite before cycling). (b) Raman spectroscopy of the graphite electrode before (bottom) and after (top) cycling.

3.2. Comparison of PC and DEGDME electrolyte systems for co-intercalation

The structural integrity of the graphite observed in Figure 2 and 4 was unexpected, considering the previous observation in PC-based lithium cells, where the graphite became severely exfoliated during the lithium–PC co-intercalation.[14, 30] To better understand these contradictory results, we performed first-principles calculations to probe the relative stability of the [lithium–solvent]$^+$ complex ions in the graphite host using different solvents. Figure 5 compares the highest occupied molecular orbital/lowest unoccupied molecular orbital (HOMO/LUMO) levels and binding energies of [Li–DEGDME]$^+$ and [Li–PC]$^+$ complex ions. The [Li–DEGDME]$^+$ complex ion exhibits a higher LUMO level than that of [Li–PC]$^+$, and importantly, the Fermi energy of graphite lies well below the LUMO level of [Li–DEGDME]$^+$ but above that of [Li–PC]$^+$. According to previous first-principles calculations, comparison of the LUMO level of a [Na–solvent$_x$]$^+$ complex and the Fermi energy of the host can hint at the relative stability of the co-intercalation.[31, 32] When the Fermi energy of the host is higher than the LUMO level of the complex, downhill electron energy transfer may occur from the graphite host to the solvent molecule, which can subsequently trigger a parasitic chemical reaction between the two components.[31, 32] This finding implies that the

$[Li–PC]^+$ complex would be unstable and possibly undergo chemical reactions with the graphite host, whereas the $[Li–DEGDME]^+$ complex would be stable in the graphite galleries (Figure 6). Furthermore, DEGDME shows stronger binding with lithium ions than PC in Figure 5, inferring more robust solvation of lithium ions in the graphite host.

Our experimental results were consistent with the prediction from the calculations. We observed that $[Li–PC]^+$ is not stable in the graphite galleries and that a substantial amount of carbon-containing gas evolved during the co-intercalation, whereas the intercalation of $[Li–DEGDME]^+$ did not induce this gas evolution. Figure 7a, b, and 8 present *in-situ* mass spectrometry analyses of the graphite electrodes with the PC and DEGDME electrolyte systems, respectively (see Figure 9 for the experimental setup). During the discharge in the Li–PC electrolyte system in Figure 7a, gas-phase byproducts such as propene, CO_2, CO, and H_2 (shaded with yellow) were clearly detected. However, no noticeable gas evolution was observed in the Li–DEGDME electrolyte system during the discharge and subsequent charge (Figure 7b), which is consistent with the observed structural integrity of the graphite electrode in the DEGDME electrolyte in Figure 4a and b. The scanning electron microscopy (SEM) results presented in Figure 10a reveal that gas evolution accompanied severe exfoliation of graphite during $[Li–PC]^+$ complex ion intercalation in graphite galleries (see Figure 11 for additional

SEM images of the exfoliated graphite using the PC-based electrolyte) unlike for the Li–DEGDME electrolyte system. Moreover, the intensity of the characteristic graphite (002) peak of the XRD pattern was significantly reduced after the cycle, as observed in Figure 10b. These results strongly suggests that the gas evolution within the graphite interlayer with the PC electrolyte could trigger the exfoliation of graphite and degradation of the crystal structure, as schematically proposed in Figure 6.

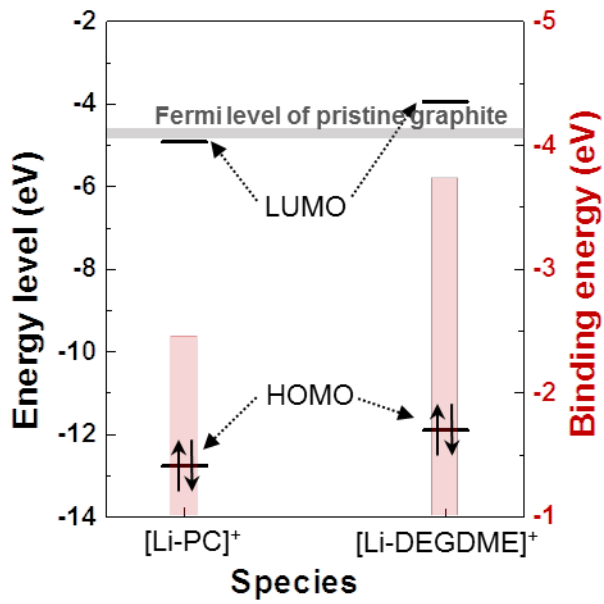

Figure 5. Comparison of LUMO and HOMO levels with the Fermi level of graphite and binding energy of lithium-solvents (left y-axis: energy level, right y-axis: binding energy).

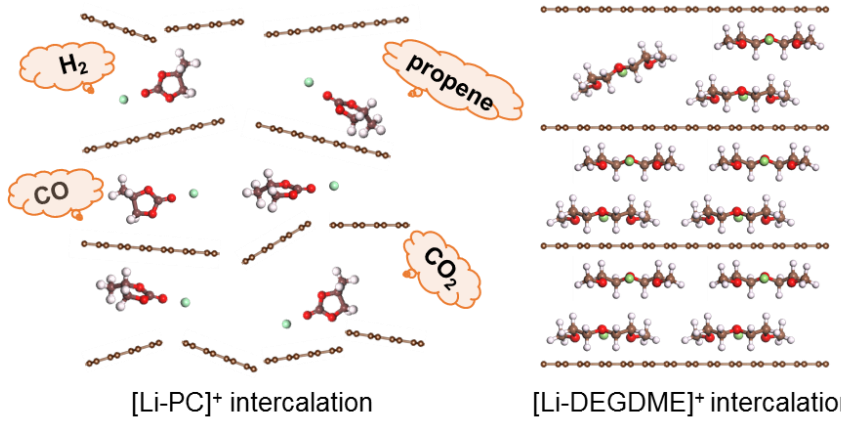

Figure 6. Schematic illustrations of lithiated graphite electrode using PC and DEGDME electrolytes.

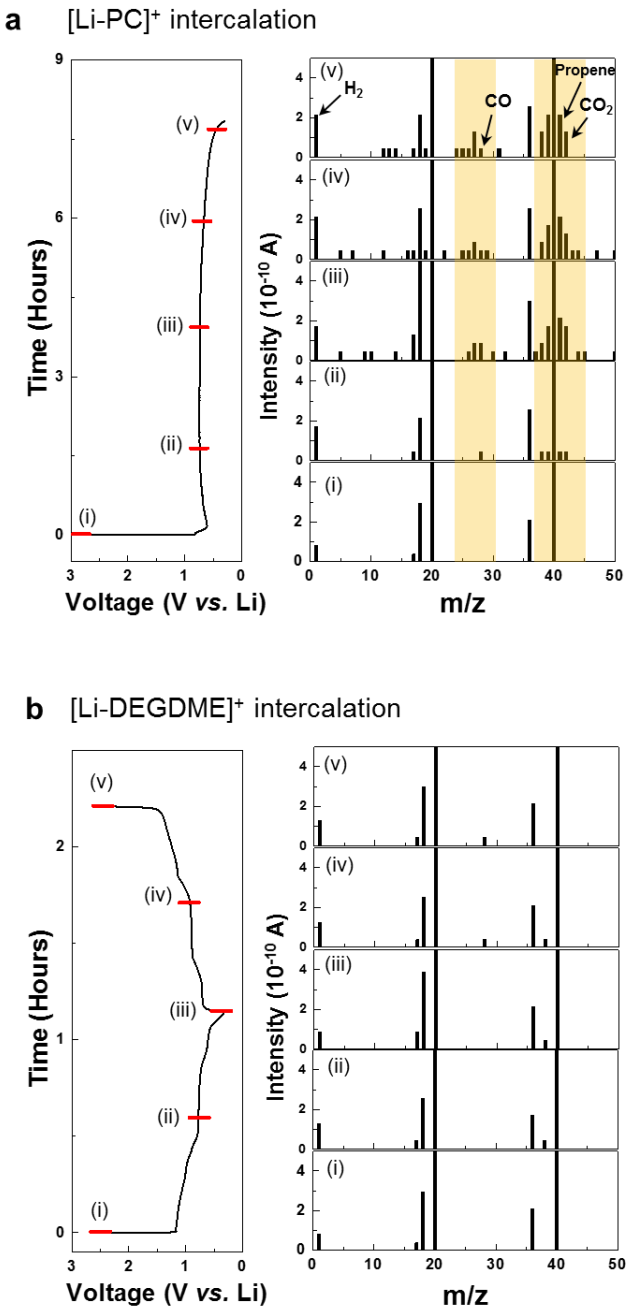

Figure 7. Gas evolution analyses during battery operations in (a) PC and (b) DEGDME electrolyte systems.

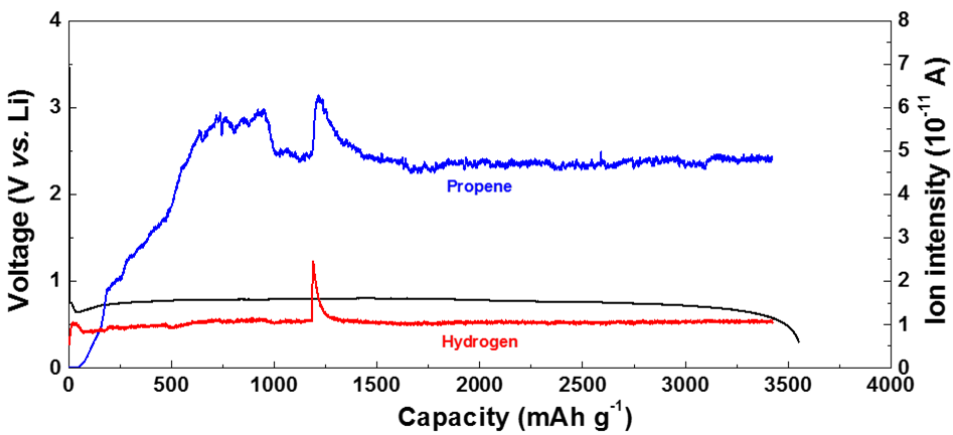

Figure 8. Differential electrochemical mass spectrometry analysis during battery operation. Graphite was used as anode active material. 1M $LiPF_6$ in PC was used as an electrolyte.

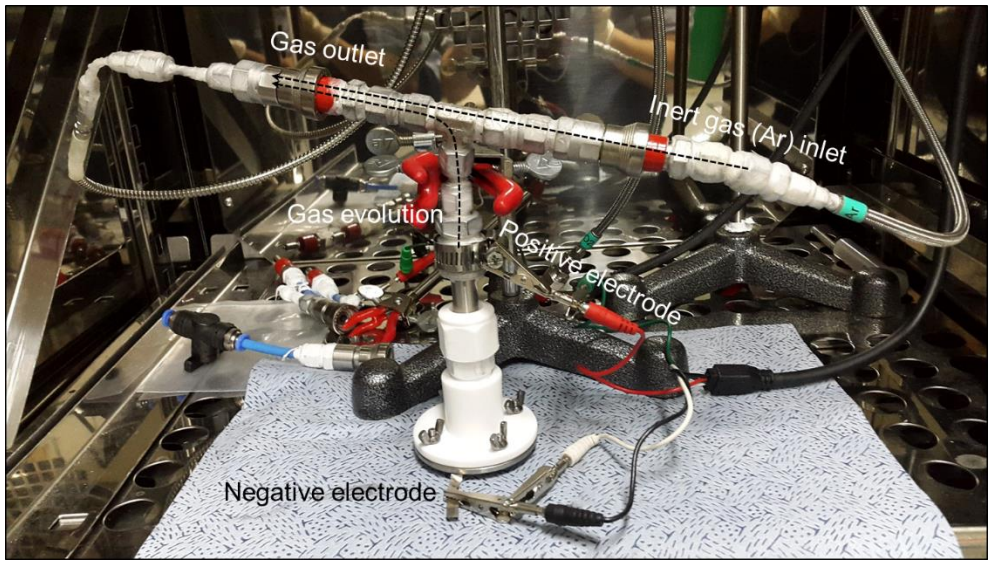

Figure 9. The configuration of *in-situ* cells for gas evolution analysis during the battery operations.

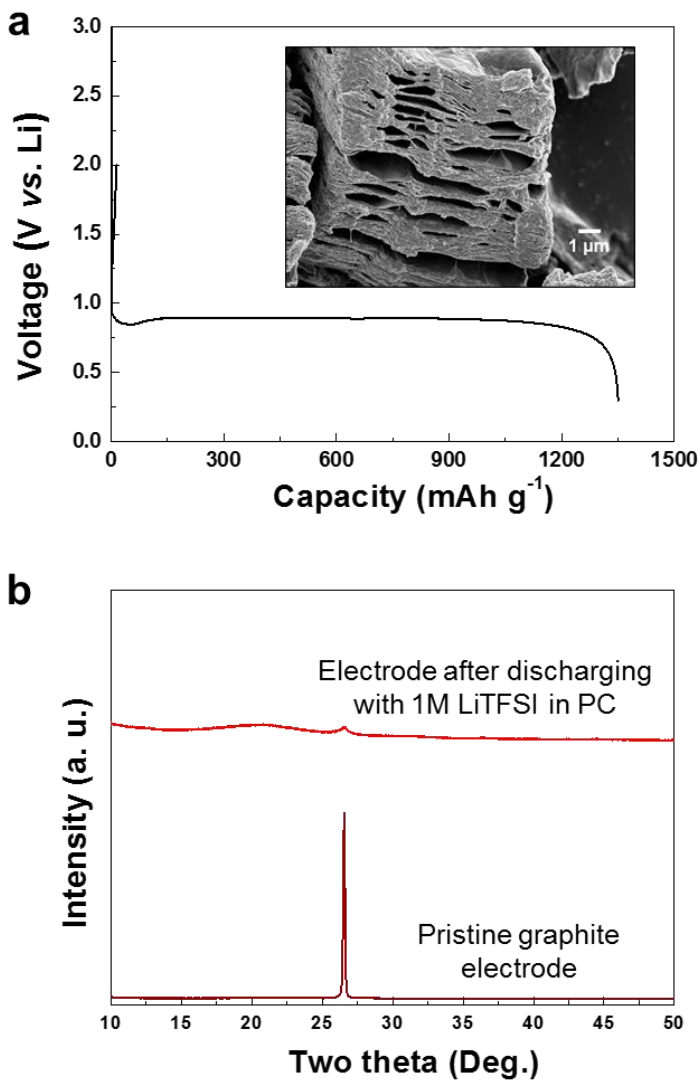

Figure 10. (a) Typical charge/discharge profile of graphite electrode using 1 M $LiPF_6$ in PC electrolyte (inset: SEM image of graphite after cycling). (b) XRD patterns of pristine graphite electrode and electrode after discharge with 1 M LiTFSI in PC.

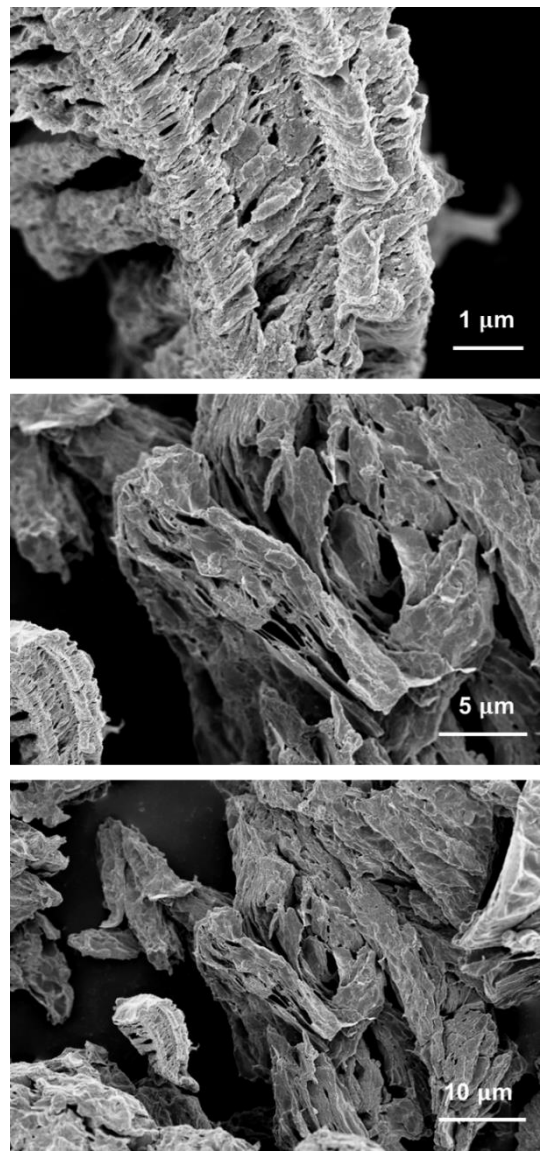

Figure 11. SEM images of graphite anode after battery operation in using 1M $LiPF_6$ in PC electrolyte.

3.3. Severe side reaction between electrolyte and lithium metal−a cause of the capacity degradation

We discovered that the observed capacity degradation for ether-based lithium cells did not originate from the degradation of the graphite electrode due to the [lithium–ether]$^+$ co-intercalation itself but simply stemmed from the degradation of the lithium metal counter electrode during the electrochemical cycling. Figure 12a reveals that the lithium metal counter electrodes were covered with dark brown films after repeated battery cycling using both LiTF and LiTFSI in DEGDME, indicating severe side reactions.[33, 34] The SEM images in Figure 12b also confirm that the surface of lithium metal was passivated by unknown byproducts after the cycling with the ether-based electrolyte. According to the energy dispersive spectroscopy (EDS) analyses in Figure 12c and d, the byproducts mainly consisted of carbon, oxygen, sulfur, and fluorine, which are the major constituting elements of the electrolyte, indicating electrolyte decomposition. Further characterization of the film using X-ray photoemission spectroscopy (XPS), as shown in Figure 12e, revealed the presence of mixed products with CF_3–O, CF_2–CH_2, O–C=O, C–O, and C–C bonding, supporting the speculation of a chemical reaction between the DEGDME and lithium metal.[34] However, no noticeable change was detected on the sodium metal

surface after the cell was cycled with the ether-based electrolyte (Figure 13). This clear difference in the metal surface suggests that the instability of the lithium metal electrode in the electrolyte caused the capacity degradation, particularly for the lithium cells. In a separate experiment, we further confirmed the chemical incompatibility of the lithium metal with the DEGDME-based electrolyte, as shown in Figure 14. The DEGDME-based electrolyte turned dark brown after being used to store lithium metal for 72 h, indicating that lithium metal is chemically unstable with DEGDME-based electrolytes, *i.e.*, 1 M LiTF and 1 M LiTFSI in DEGDME. In contrast, no significant changes were observed for carbonate-based electrolytes, *i.e.*, 1 M lithium hexaflourophosphate ($LiPF_6$) in ethylene carbonate/dimethylene carbonate (EC/DMC) and 1 M LiTFSI in EC/DMC, in the same experiment (Figure 14). Based on these results, a graphite/lithium metal cell was assembled with 1M LiTFSI in DEGDME and rested it for 72 hours, followed by charging/discharging (Figure 15). It revealed that the capacity decreases much more rapidly in the 72 hour rested cell than the immediately cycled cell (Figure 1c), confirming again that capacity degradation is attributable to the severe side reaction between lithium metal and the electrolyte. The incompatibility of lithium metal with the DEGDME electrolyte in the electrochemical cell was additionally confirmed for lithium metal cells employing a $Li_4Ti_5O_{12}$ (LTO) electrode (*vs*. lithium metal electrode), which

underwent rapid capacity degradation, as observed in Figure 16. Inspired by this finding, we attempted to minimize the chemical reaction between the DEGDME-based electrolyte and lithium metal and re-investigated the cycling performance of the graphite electrode based on the co-intercalation. Figure 17 compares the cycle properties of graphite electrode cells with and without lithium nitrate ($LiNO_3$) additives in the electrolyte. The addition of $LiNO_3$ results in a chemical protection layer on the lithium metal surface against the electrolyte after the initial battery cycling.[35, 36] The cycle performance was significantly enhanced with the $LiNO_3$ additive, providing further evidence of the chemical reaction between the DEGDME-based electrolyte and lithium metal in the previously observed rapid capacity degradation of electrochemical cells containing the co-intercalating graphite electrode.

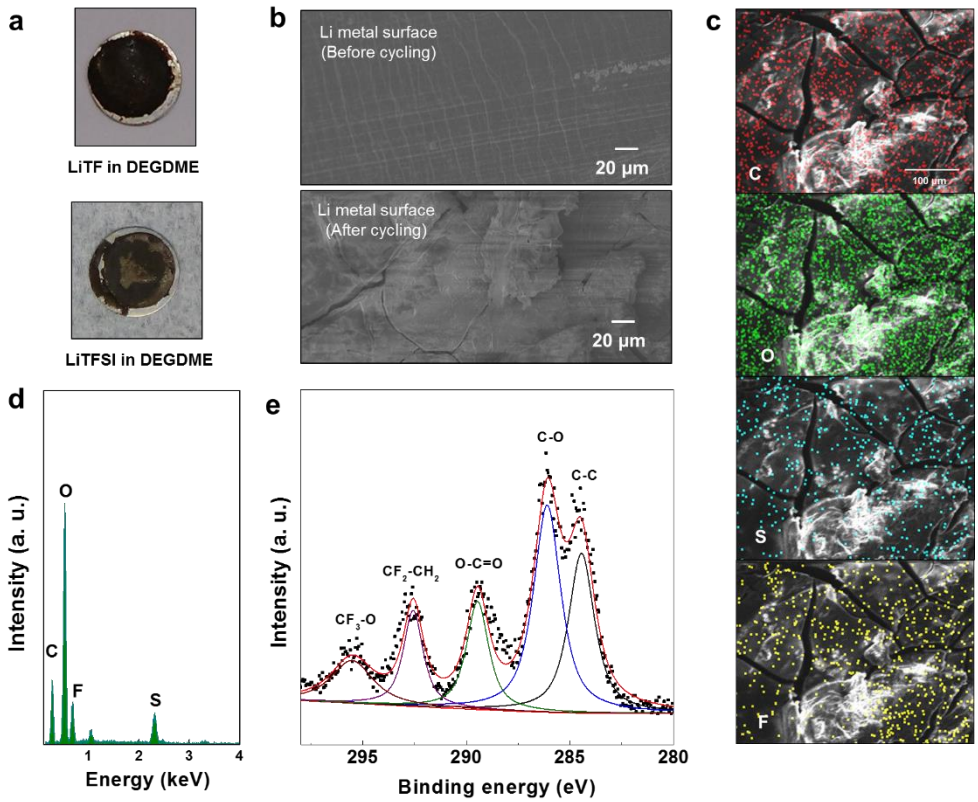

Figure 12. Photo-images of lithium metal and separators after battery operation in (a) 1 M LiTF in DEGDME (top) and 1 M LITFSI in DEGDME (bottom) electrolytes. (b) SEM images of lithium metal before and after battery operation. (c) EDS mapping, (d) EDS spectrum, and (e) XPS analyses of lithium metal after battery operation with 1 M LiTFSI in DEGDME.

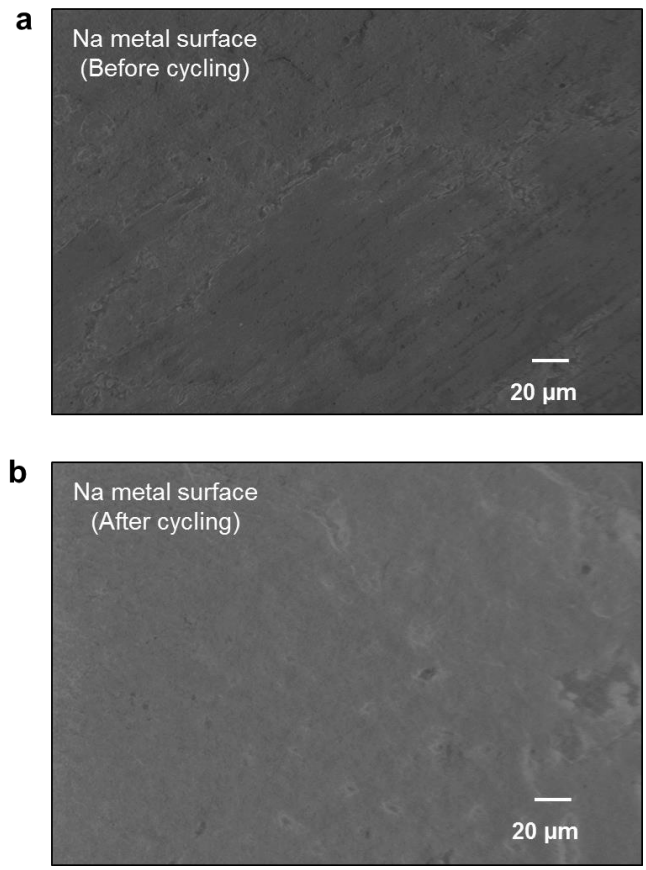

Figure 13. SEM images of sodium metal (a) before and (b) after cycling with 1M $NaPF_6$ in DEGDME electrolyte.

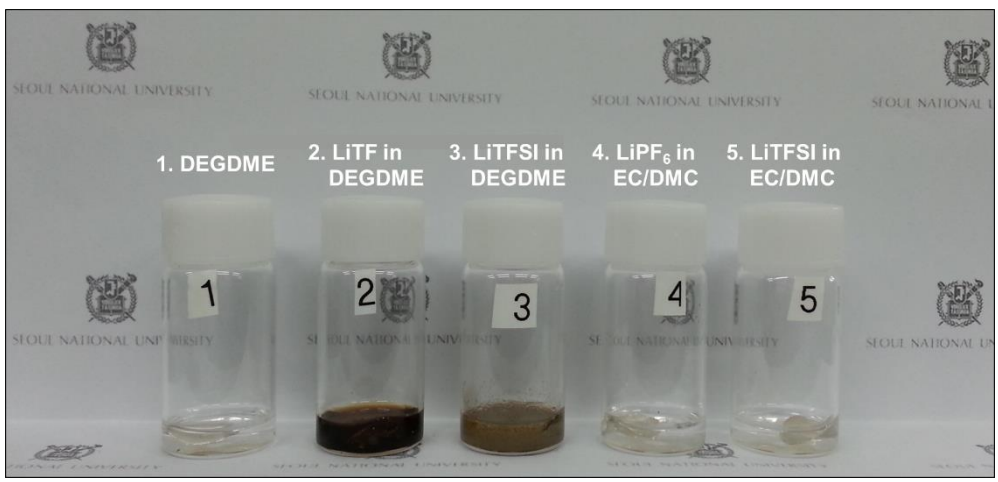

Figure 14. Photo-images of the electrolytes (1. DEGDME, 2. 1M LiTF in DEGDME, 3. 1M LiTFSI in DEGDME, 4. 1M $LiPF_6$ in EC/DMC, and 5. 1M LiTFSI in EC/DMC) after lithium metal storage for 72 hours.

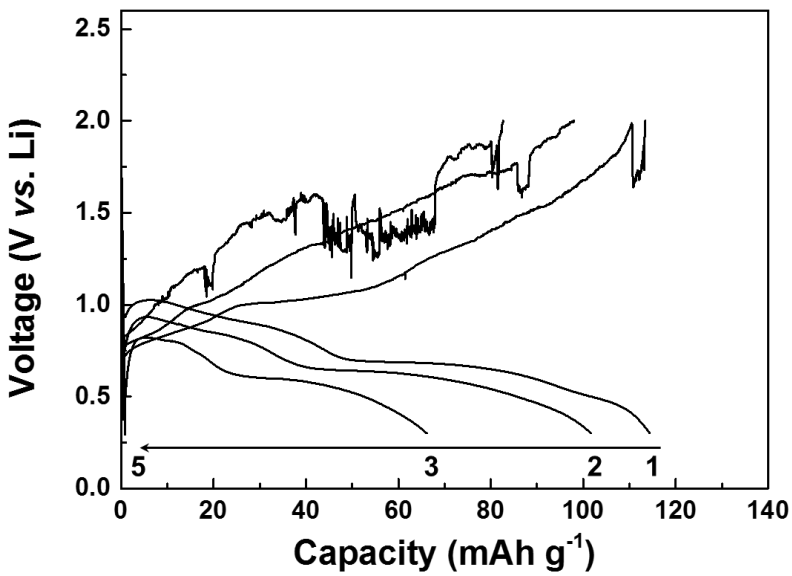

Figure 15. Charge/discharge profiles of graphite/lithium cells using 1M LiTFSI in DEGDME electrolyte after 72 hour rest. The capacity decreases more rapidly than the immediately cycled cell (Figure 1c).

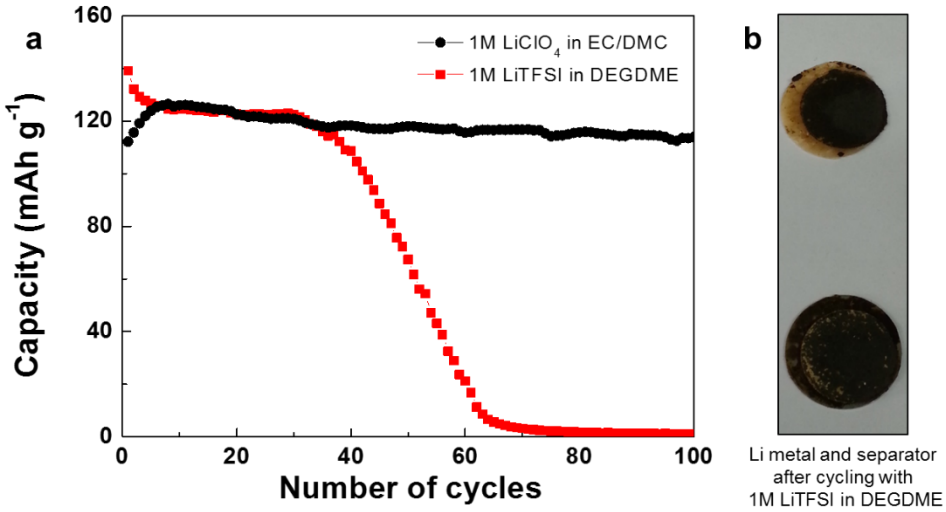

Figure 16. (a) Cycle performance of $Li_4Ti_5O_{12}$ anode in lithium half-cells with 1M lithium perchlorate ($LiClO_4$) in EC/DMC and 1M LiTFSI in DEGDME. (b) Photo-images of lithium metal and separator after cycling with 1M LiTFSI in DEGDME electrolyte.

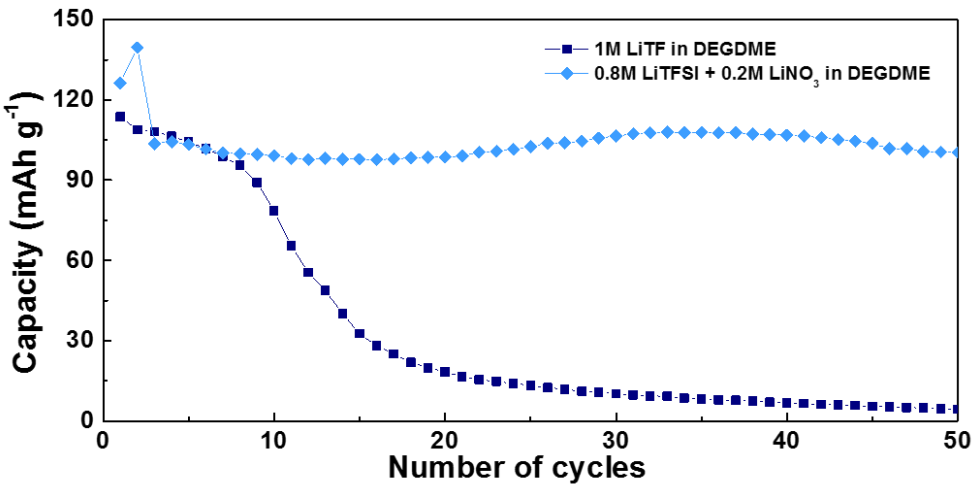

Figure 17. Cycle stability of the graphite/lithium cells with and without $LiNO_3$ additive.

3.4. High power capability of co-intercalation

The electrochemical property of the graphite electrode based on the co-intercalation is further explored in Figure 18 and 20. First, to verify the practical feasibility of the graphite co-intercalation, a full cell was assembled with a $LiFePO_4$ (LFP) cathode and graphite anode in a DEGDME-based electrolyte. Figure 18a presents typical charge/discharge profiles of the cell, which demonstrate that the characteristic profiles of both $LiFePO_4$ and graphite were observed in the full cell and were not altered upon repeated battery cycling. In addition, no color change indicating side reaction was observed in the separator of the graphite/LFP cell whereas the separator of graphite/lithium metal cell turned black (Figure 19). The full cell retained approximately 80% of the initial discharge capacity even after 200 cycles (Figure 18b), validating that the $[Li–DEGDME]^+$ complex ion intercalation in the graphite is highly reversible and applicable as a full cell. To further understand the co-intercalation, the electrochemical performance of the graphite electrode was compared with that of conventional lithium-ion intercalation, as shown in Figure 20a and b. Despite the fact that the theoretical capacity of $[Li\text{-}DEGDME]^+$ complex co-intercalation is lower than that of conventional lithium-ion intercalation probably due to the space occupancy of the lithium solvating molecules in graphite galleries, the co-

intercalation-based reaction was capable of delivering a much higher power capability than the conventional lithium ion intercalation using graphite with an ~100-μm particle size. The $[Li–DEGDME]^+$ co-intercalation into the graphite could be performed up to 1 A g^{-1} (charge time < 6 min) without a significant reduction of the capacity, which is consistent with our previous findings.[26] In contrast, a negligible capacity was achieved for the conventional lithium ion intercalation at 1 A g^{-1}. Figure 20c plots the specific capacities of the two cells as a function of the current rates. Although the normal lithium ion intercalation into graphite delivered higher capacity than the co-intercalation at low current densities, the capacity decreased dramatically with increasing current rate. However, the deliverable capacity from the co-intercalation remained nearly constant irrespective of the current rates and even exceeded that of the conventional lithium ion intercalation for currents greater than 0.5 A g^{-1}. The faster kinetics of the co-intercalation into graphite is also supported by the smaller increase in the polarization between the charge and discharge with increasing current in Figure 20d. At low current rates, the polarizations were almost identical for both cases; however, the polarization of the co-intercalation became much lower at high current rates. At the 1 A g^{-1} rate, the polarization between the charge and discharge was as low as 0.3 V for the co-intercalation, which is only half of the value for the normal lithium ion intercalation. In Figure 20e, the rate capability is

compared in terms of the normalized capacity retention, demonstrating that the co-intercalation is capable of retaining approximately 87% of the theoretical capacity at 1 A g^{-1}. For a more practical feasibility comparison, we assessed the energy densities for the co-intercalation and normal intercalation in the full cell setup with $LiFePO_4$ as a cathode (Figure 21). The gravimetric/volumetric energy density of the co-intercalation eventually exceeded that of the conventional intercalation at current rates above 0.5 A g^{-1}, highlighting the viability of the co-intercalation-based graphite electrode for high-power energy storage devices, even with a slightly higher electrolyte price of ether-based electrolyte (Table 1). However, it should be noted that the electrolyte accounts for approximately 8% of the total battery price,[37] thus it is believed that the cost difference would not be substantial. Additionally, the energy density of $[Li\text{-}DEGDME]^+$ co-intercalation was compared with $Li_4Ti_5O_{12}$, a widely known electrode material for its high power capability. $[Li\text{-}DEGDME]^+$ co-intercalation exhibits similar gravimetric energy density compared to $Li_4Ti_5O_{12}$, but it was found that the co-intercalation graphite is capable of providing more merits in delivering higher practical volumetric energy density than $Li_4Ti_5O_{12}$ considering all cell components including conductive agents, binder and current collector (Figure 21). While there were not particular difference regarding the binder and the current collector, a larger amount of conducting agent was inevitable to

prepare the LTO electrode owing to its intrinsic low electronic conductivity compared to the graphite. Both full cells showed stable cycle life as demonstrated in Figure 22. Note that the high power capability of the graphite electrode can be beneficial to the safety of batteries. In conventional lithium-ion batteries, graphite can pose a safety issue during a fast lithiation process; the overpotential arising from the high current can lead to lithium metal plating on the electrode, which is highly detrimental.[38, 39] The fast insertion kinetics of the co-intercalation in graphite can be considered a merit to prevent such situations. Moreover, the relatively high redox potential (> 0.3 V *vs*. Li) of the co-intercalation, far greater than the lithium metal formation potential, further precludes lithium metal plating,[21] which was also experimentally confirmed by surface observation of graphite using SEM after fast discharging (Figure 23). As will be discussed later, the lack of thick SEI layers on the graphite anode cycled with the ether-based electrolyte also aids in enhancing the safety properties of a graphite anode using co-intercalation.[40, 41]

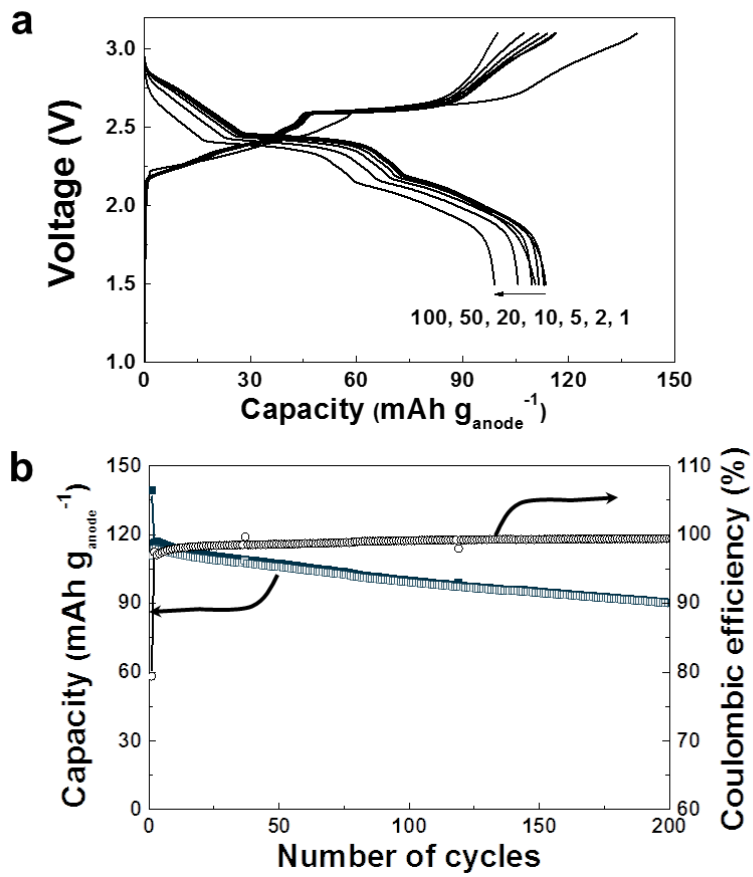

Figure 18. (a) Charge/discharge profiles and (b) cycle stability of $LiFePO_4$/graphite cells.

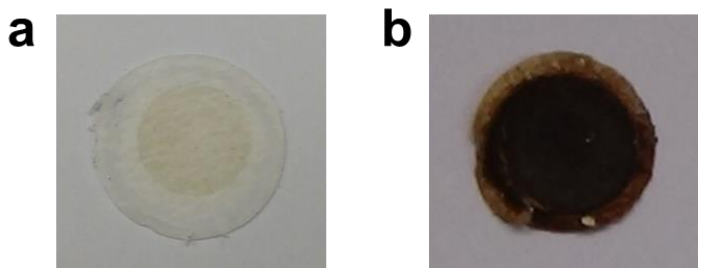

Figure 19. Images of separators cycled with 1M LiTFSI in DEGDME for 100 cycles. The cells were assembled with (a) graphite/LFP and (b) graphite/lithium metal.

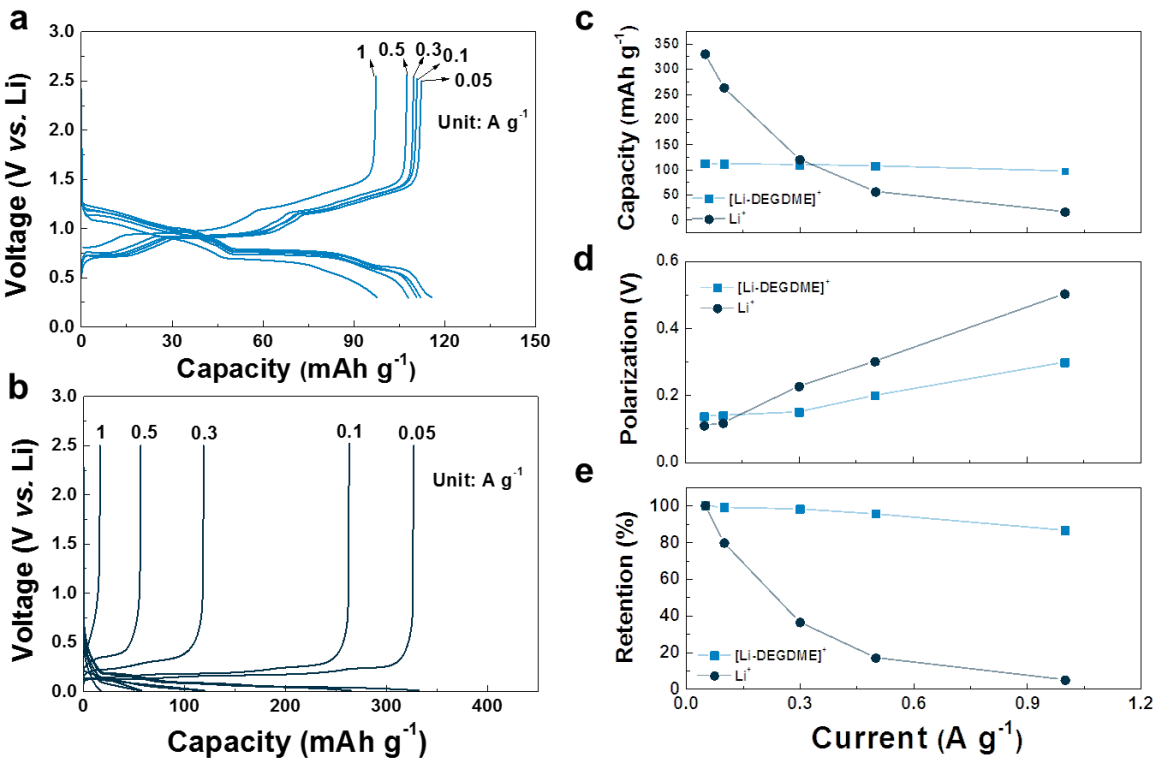

Figure 20. Rate capability of the graphite electrode in (a) 1 M LiTFSI in DEGDME and (b) 1 M $LiPF_6$ in EC/DMC (1:1 *vol.*) electrolytes. Comparison of rate capability in terms of (e) capacity, (f) polarization, and (g) capacity retention.

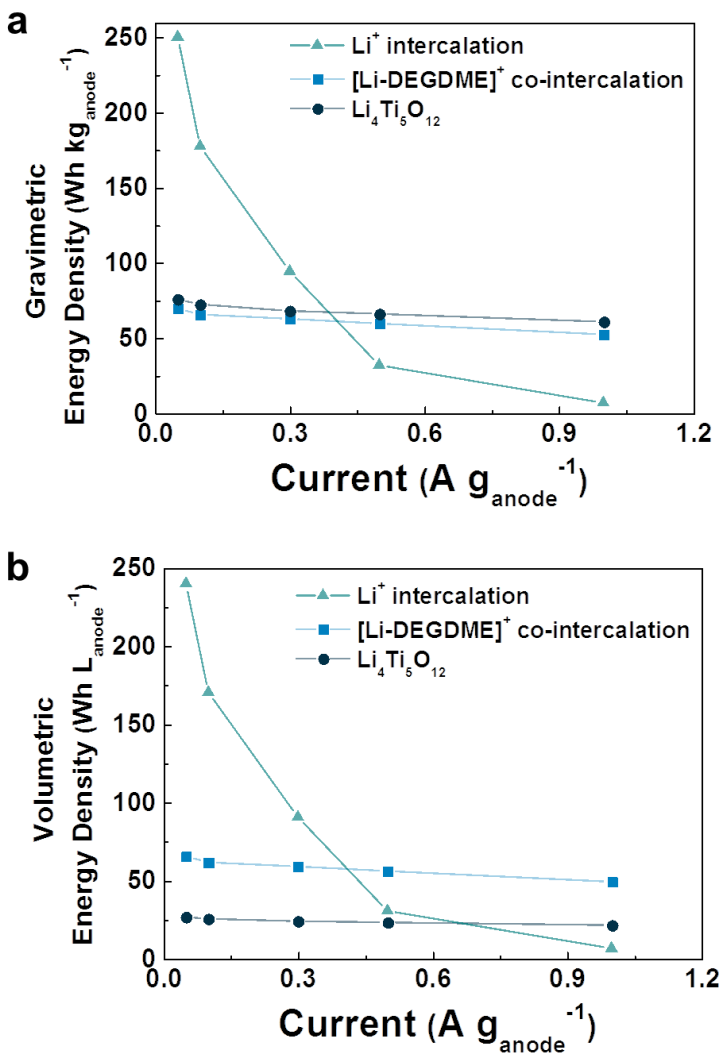

Figure 21. Energy densities of the cells in terms of (a) gravimetric energy density and (b) practical volumetric energy density including the conductive agents, binder and the current collector. Note that the full cells were constructed with excessive amount of $LiFePO_4$ cathode for a fixed voltage.

Table 1. Prices of the two types of electrolytes. Note that the prices came from the domestic electrolyte manufacturer on April 1, 2017, but the name of the company was closed at the request of the manufacturer.

	1M $LiPF_6$ in EC/DMC (1:1 *vol.*)	1M LiTFSI in DEGDME
Price [\$ kg^{-1}]	133.27	222.12

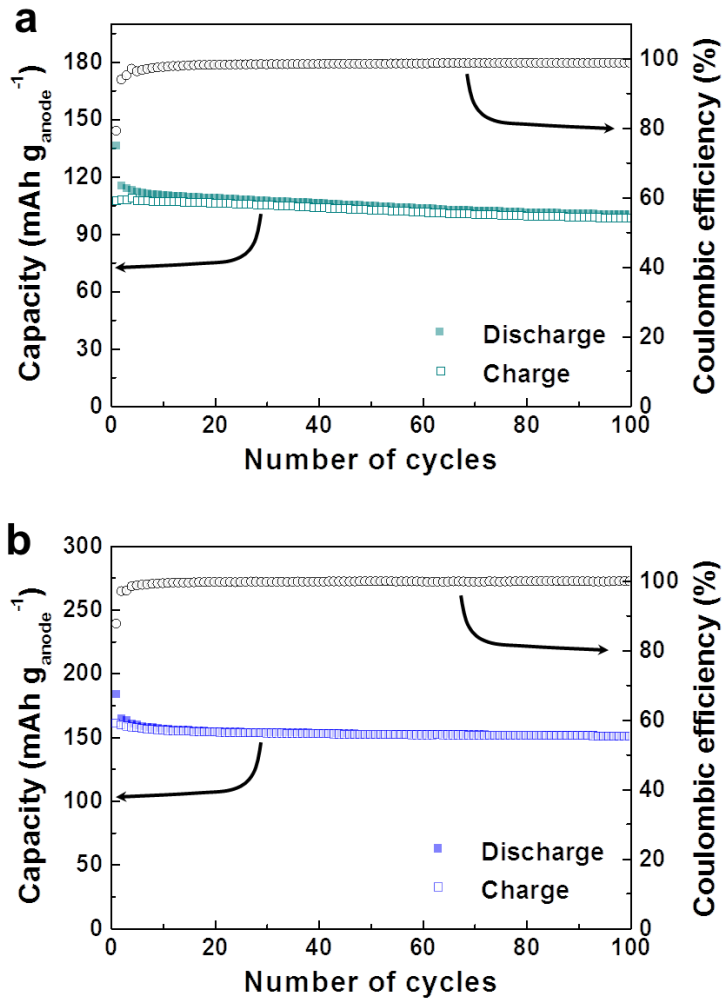

Figure 22. Cycle life of the full cells of (a) graphite/LFP and (b) LTO/LFP with 1M LiTFSI in DEGDME electrolyte.

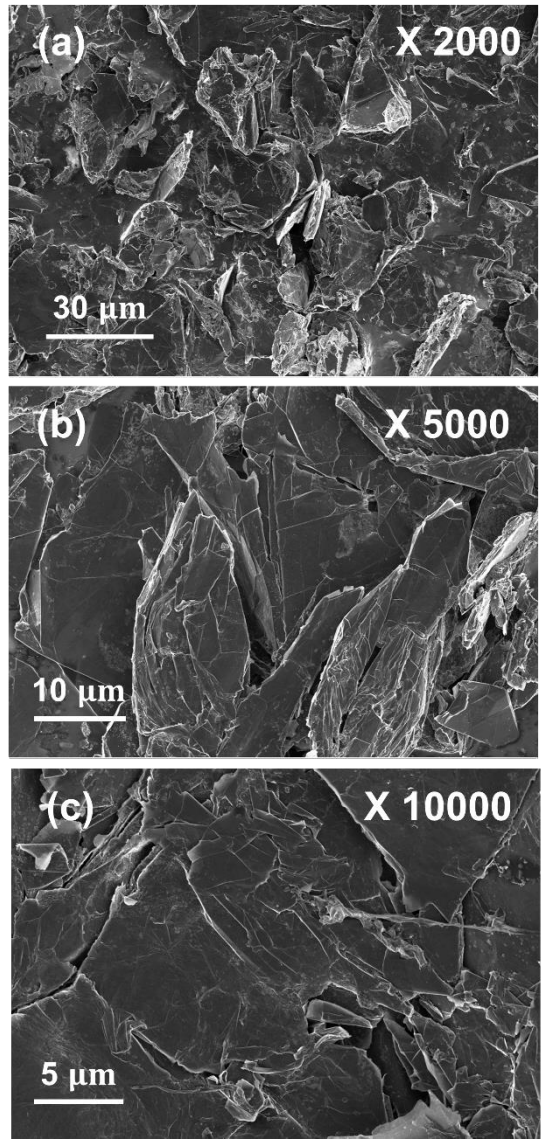

Figure 23. SEM images of graphite after discharging at a current density of 1A g^{-1}. (a) 2000, (b) 5000, and (c) 10,000 times magnification.

3.5. Origin of high rate capability for co-intercalation

The high rate capability of $[Li–DEGDME]^+$ complex ion intercalation in the graphite electrode is unusual considering the large size of the complex ion. To better understand this phenomenon, we considered the possible factors assisting the fast complex ion intercalation kinetics in graphite. In general, guest ion intercalation in electrochemical cells occurs in the following four steps: (i) guest ion diffusion in the electrolyte, (ii) desolvation process at the interface between the electrolyte and electrode, (iii) guest ion diffusion through the SEI layer, and (iv) bulk diffusion in the active electrode material.[42] For (i), we simply compared the ionic conductivities of 1 M LiTFSI in EC/DMC and DEGDME (see the Experimental section for detailed information). According to our measurements, the ionic conductivities of the two electrolytes were 10.75 ± 0.99 and 9.56 ± 0.16 mS cm^{-1}, respectively, which are consistent with previous reports.[43, 44] The marginally similar ionic conductivities indicate that the ionic conductivity of the electrolyte is not a determining factor for the distinctive kinetics. To estimate the effect of (ii), the energy barriers of the desolvation process were comparatively calculated for DEGDME, DMC, and EC solvations (Figure 24). The desolvation energy was estimated based on the energy required for a lithium ion to remove a solvent molecule (see the Experimental section for

a detailed description of the calculations).[45, 46] Each step in Figure 24 represents the series of energies required to desolvate the multiple solvation shells. For example, in the bottom panel of Figure 24, $[Li–2EC]^+$ represents a lithium ion solvated by two EC molecules, and 1.748 eV is the energy necessary to remove one EC molecule and form $[Li–EC]^+$. The first solvation (or last desolvation) energy is significantly higher for DEGDME (3.730 eV) than for DMC (2.091 eV) or EC (2.384 eV), indicating that the lithium ion and DEGDME solvent are strongly bound to each other, promoting the co-intercalation.[31] This finding is consistent with the experimentally observed $[Li–DEGDME]^+$ co-intercalation phenomena in graphite. Thus, we considered the second-last energy barrier in the DEGDME system to be the effective desolvation energy (1.434 eV), whereas the last energy barriers with the highest values were considered the desolvation energies for DMC (2.091 eV) and EC (2.384 eV) because of their conventional intercalation (highlighted in red in Figure 24). The energies required to desolvate EC or DMC solvents are much higher than that of DEGDME solvent desolvation by approximately 0.7–1 eV, which implies that the desolvation of lithium ions in EC or DMC for the intercalation of graphite will be relatively slower than the desolvation kinetics of the co-intercalation in DEGDME.

We further characterized the SEI layers of the graphite electrodes, which can affect the intercalation kinetics, using transmission electron

microscopy (TEM) and XPS. Interestingly, the TEM results indicated that no noticeable SEI layer was formed at the surface of the graphite cycled with 1 M LiTFSI in DEGDME (Figure 25a), whereas a thick amorphous-like SEI layer was commonly observed at the surface of graphite cycled with 1 M LiTFSI in EC/DMC (Figure 25b). The XPS results with depth profiling also clearly confirmed that the SEI layer does not form on the surface of the graphite anode in the DEGDME electrolyte system (Figure 25c). This result contrasts with that for the EC/DMC electrolyte system (Figure 25d), which has typical compounds constituting the SEI such as Li_2CO_3 or $(CH_2OCO_2Li)_2$ and C–O-containing materials.[41] It is believed that the absence of the surface film for the co-intercalation is partly due to the relatively high voltage cut-off of the co-intercalation in the discharge (0.3 V *vs.* Li) and the high LUMO level of the ether solvent, which prevents the reduction of the electrolyte. This result is similar to that for a LTO electrode, which does not generally form a surface film when used as an anode because of its high redox potential.[47, 48] Moreover, we speculate that the absence of an apparent desolvation process in the co-intercalation may have contributed to preventing the formation of thick SEI layers; however, further investigation is necessary. The lack of the typical SEI layers at the surface would enable the facile transport of $[\text{lithium–ether}]^+$ complex ions into the graphite.

Finally, to understand the bulk diffusion in the electrode during the electrochemical reaction, we probed the electrochemical response of the [lithium–ether]$^+$ complex ion intercalation using cyclic voltammetry (CV) with scan rates from 0.2 to 3 mV s^{-1}, as shown in Figure 26a. Here, it was assumed that the scan rate and peak current follow a power-law equation:

$$i=av^b,$$

where i is the measured peak current, v is the voltage sweep rate, and a and b are adjustable parameters.[49] A b value of 0.5 generally indicates a diffusion-controlled reaction, whereas a b value of 1 indicates a capacitive reaction.[50] We calculated the b values of every peak in the [lithium–ether]$^+$ complex intercalation by plotting log (scan rate) versus log (peak current), as shown in Figure 26b. To our surprise, a significant pseudocapacitive nature was revealed for the [lithium–ether]$^+$ complex intercalation, in contrast to the charge storage behavior of conventional lithium ion intercalation, which is mostly diffusion controlled.[51] The b values of the peaks were estimated to be 0.99, 0.87, 0.61, and 0.58, respectively, indicating a mixed pseudocapacitive and diffusion reaction, or previously reported partial intercalation pseudocapacitance, during the electrochemical response.[52-56] Considering the apparent first-order phase transition of the [lithium–ether]$^+$ complex in the bulk graphite, as evidenced in the *ex-situ* XRD patterns in Figure 1d, the precise origin of this behavior has not yet been clearly

understood. However, this behavior implies that [lithium–ether]$^+$ complex ion diffusion in the graphite galleries promotes faster kinetics compared to conventional lithium ion intercalation. The enlarged space of the co-intercalated graphite with a large amount of the [lithium–ether]$^+$ complex might have a similar lithium insertion local environment to those of the expanded graphite or restacked graphene, which may induce the pseudocapacitive behavior for the intercalation. Also, similar observations have been reported in such as mesoporous MoS_2,[52] MoO_{3-x},[53] MoS_2 nanocrystal,[54] nanosized-MoO_2,[55] and TiS_2 nanocrystals,[56] which were ascribed to the intercalation pseudocapacitance resulting from the suppressing intercalation-induced phase transitions. In addition, we speculate that the unusually large distance between graphene layers triggered by the initial co-intercalation of the [lithium–ether]$^+$ complex promotes the subsequent co-intercalation of the complex ions with a non-limited diffusion nature. In this case, the [lithium–ether]$^+$ co-intercalation would exhibit a capacitive behavior with much improved kinetics, which is similar to the unusually fast charge storage mechanism and CV response demonstrated by Dunn *et al.* for an orthorhombic Nb_2O_5 electrode.[50]

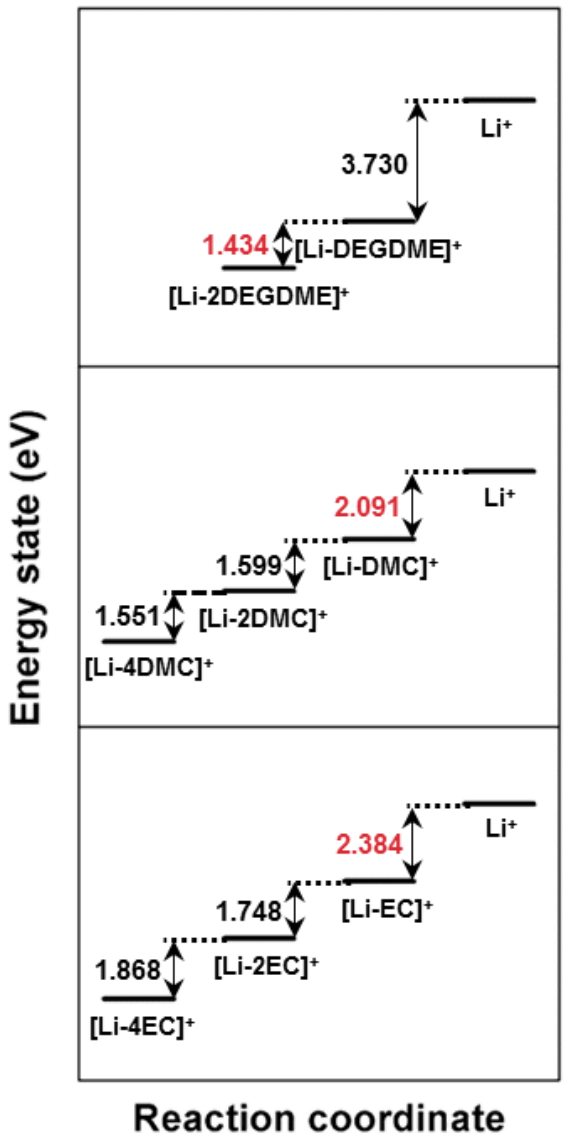

Figure 24. Desolvation energy of Li ion solvated with EC, DMC, and DEGDME.

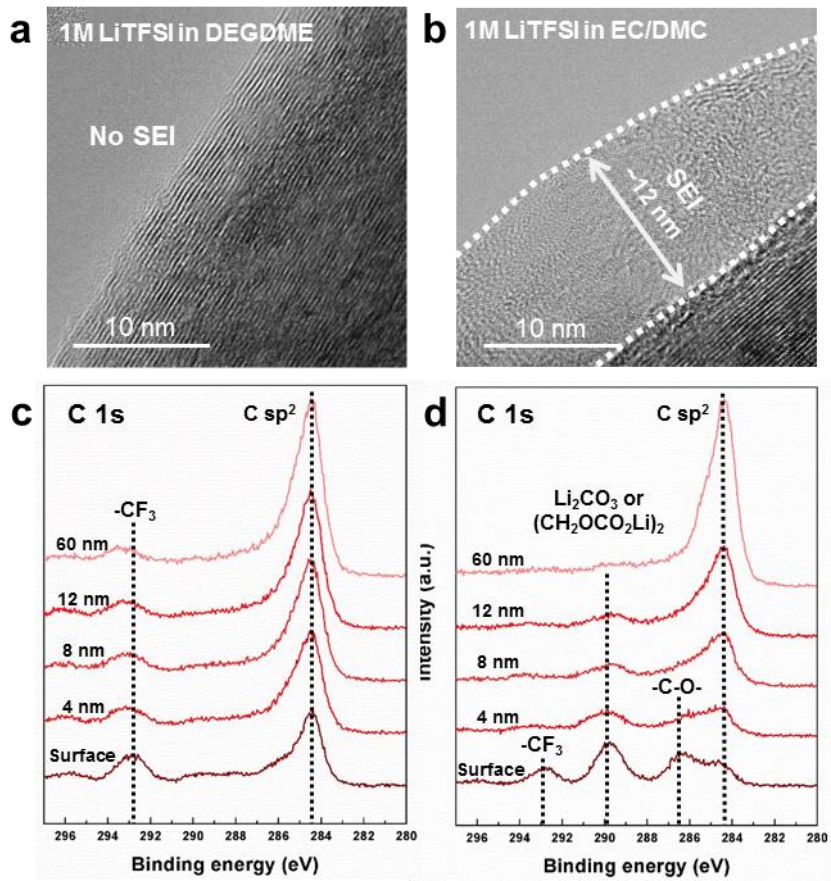

Figure 25. (a–b) TEM images and (c–d) XPS analyses characterizing the edge of graphite cycled with 1 M LiTFSI in DEGDME (left) and 1 M LiTFSI in EC/DMC (1:1 vol.) (right). The XPS CF3 signal originates from the poly(vinylidene) fluoride binder.

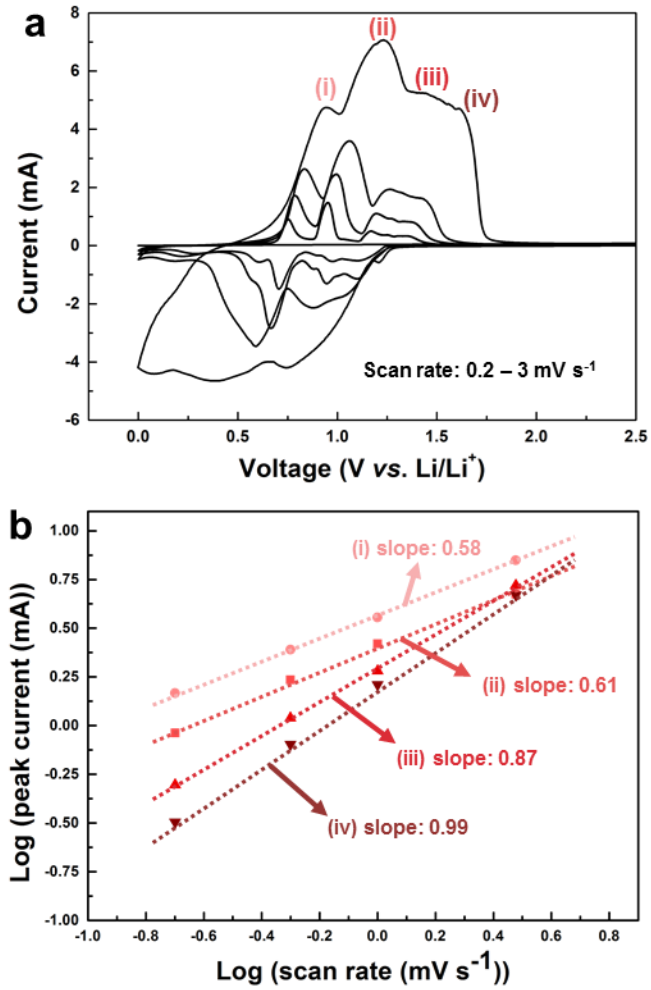

Figure 26. (a) CV profile of natural graphite using 1 M LiTFSI in DEGDME electrolyte. (b) Anodic peak current dependence on the scan rate derived from CV and used to determine the capacitive and intercalation contributions to energy storage.

4. Conclusion

We demonstrated for the first time that lithium ion/solvent co-intercalation into a graphite electrode can be highly reversible in lithium cells, which can exhibit promising electrochemical performance with unexpected high power capability. The chemical compatibility of the solvent molecule with the pristine graphite was shown to critically affect the stable co-intercalation. Furthermore, we revealed that the severe capacity degradation previously observed for co-intercalation in a graphite electrode does not stem from the co-intercalation itself but simply results from the chemical instability of the lithium metal in the ether-based electrolyte system. Accordingly, complex ion co-intercalation in a graphite electrode was successfully utilized in both half cells with protected lithium metal and full cells with excellent reversibility. Compared with conventional lithium ion intercalation, the graphite electrode based on the co-intercalation was capable of delivering an impressively higher power capability, retaining more than 87% of its theoretical capacity at a current density of 1 A g^{-1} without the risk of lithium metal plating. Based on combined first-principles calculations and experiments, this higher power capability was attributed to faster desolvation kinetics, the negligible presence of a SEI layer on the graphite electrode, and the diffusion-less charge storage mechanism. Considering the high power

capability and expected safety enhancement, co-intercalation-based graphite electrodes may offer an alternative direction for the utilization of graphite in high-power lithium-ion batteries, and this work constitutes the first step toward this advancement.

5. References

[1] L. B. Ebert, Ann. Rev. Mater. Sci. 1976, 6, 181.

[2] Y. Nishi, J. Power Sources 2001, 100, 101.

[3] F. Cao, I. V. Barsukov, H. J. Bang, P. Zaleski, J. Prakash, J. Electrochem. Soc. 2000, 147, 3579.

[4] M. Yoshio, H. Wang, K. Fukuda, Angew. Chem. 2003, 115, 4335.

[5] T. Tsumura, A. Katanosaka, I. Souma, T. Ono, Y. Aihara, J. Kuratomi, M. Inagaki, Solid State Ionics 2000, 135, 209.

[6] Y. Kobayashi, H. Miyashiro, K. Kumai, K. Takei, T. Iwahori, I. Uchida, J. Electrochem. Soc. 2002, 149, A978.

[7] D. Aurbach, E. Zinigrad, Y. Cohen, H. Teller, Solid State Ionics 2002, 148, 405.

[8] J.-i. Yamaki, H. Takatsuji, T. Kawamura, M. Egashira, Solid State Ionics 2002, 148, 241.

[9] M. Winter, G. H. Wrodnigg, J. O. Besenhard, W. Biberacher, P. Novák, J. Electrochem. Soc. 2000, 147, 2427.

[10] M. Ishikawa, T. Sugimoto, M. Kikuta, E. Ishiko, M. Kono, J. Power Sources 2006, 162, 658.

[11] D. Aurbach, Y. Ein-Eli, B. Markovsky, A. Zaban, S. Luski, Y. Carmeli, H. Yamin, J. Electrochem. Soc. 1995, 142, 2882.

[12] R. McMillan, H. Slegr, Z. X. Shu, W. Wang, J. Power Sources 1999, 81–82, 20.

[13] P. Arora, R. E. White, M. Doyle, J. Electrochem. Soc. 1998, 145, 3647.

[14] B. P. Sullivan, J. Electrochem. Soc. 1970, 117, 222.

[15] M. Arakawa, J.-I. Yamaki, J. Electroanal. Chem. Interf. Electrochem. 1987, 219, 273.

[16] H. Moon, R. Tatara, T. Mandai, K. Ueno, K. Yoshida, N. Tachikawa, T. Yasuda, K. Dokko, M. Watanabe, J. Phys. Chem. C 2014, 118, 20246.

[17] Y. Yamada, K. Usui, C. H. Chiang, K. Kikuchi, K. Furukawa, A. Yamada, ACS Appl. Mater. Interf. 2014, 6, 10892.

[18] T. Abe, N. Kawabata, Y. Mizutani, M. Inaba, Z. Ogumi, J. Electrochem. Soc. 2003, 150, A257.

[19] X.-R. Liu, L. Wang, L.-J. Wan, D. Wang, ACS Appl. Mater. Interf. 2015, 7, 9573.

[20] H. Kim, J. Hong, Y.-U. Park, J. Kim, I. Hwang, K. Kang, Adv. Funct. Mater. 2015, 25, 534.

[21] B. Jache, P. Adelhelm, Angew. Chem. Int. Edit. 2014, 53, 10169.

[22] Z. Zhu, F. Cheng, Z. Hu, Z. Niu, J. Chen, J. Power Sources 2015, 293, 626.

[23] B. Jache, J. O. Binder, T. Abe, P. Adelhelm, Phys. Chem. Chem. Phys. 2016, 18, 14299.

[24] P. Han, X. Han, J. Yao, L. Zhang, X. Cao, C. Huang, G. Cui, J. Power Sources 2015, 297, 457.

[25] P. Han, X. Han, J. Yao, Z. Liu, X. Cao, G. Cui, Electrochem. Commun. 2015, 61, 84.

[26] H. Kim, G. Yoon, K. Lim, K. Kang, Chemical Communications 2016.

[27] C. Gejke, L. Börjesson, K. Edström, Electrochem. Commun. 2003, 5, 27.

[28] A. M. Andersson, M. Herstedt, A. G. Bishop, K. Edström, Electrochim. Acta 2002, 47, 1885.

[29] H. Kim, J. Hong, G. Yoon, H. Kim, K.-Y. Park, M.-S. Park, W.-S. Yoon, K. Kang, Energ. Environ. Sci. 2015, 8, 2963.

[30] G. C. Chung, H. J. Kim, S. I. Yu, S. H. Jun, J. w. Choi, M. H. Kim, J. Electrochem. Soc. 2000, 147, 4391.

[31] G. Yoon, H. Kim, I. Park, K. Kang, Adv. Energy Mater. 2016, 1601519.

[32] M. Shiraishi, M. Ata, Carbon 2001, 39, 1913.

[33] Y. Yamada, A. Yamada, J. Electrochem. Soc. 2015, 162, A2406.

[34] J. Qian, W. A. Henderson, W. Xu, P. Bhattacharya, M. Engelhard, O. Borodin, J.-G. Zhang, Nat. Commun. 2015, 6, 6362.

[35] D. Aurbach, E. Pollak, R. Elazari, G. Salitra, C. S. Kelley, J. Affinito, J. Electrochem. Soc. 2009, 156, A694.

[36] X. Liang, Z. Wen, Y. Liu, M. Wu, J. Jin, H. Zhang, X. Wu, J. Power Sources 2011, 196, 9839.

[37] Y. Kim, K.-H. Ha, S. M. Oh, K. T. Lee, Chemistry – A European Journal 2014, 20, 11980.

[38] A. Same, V. Battaglia, H.-Y. Tang, J. Park, J. Appl. Electrochem. 2012, 42, 1.

[39] I. Belharouak, G. M. Koenig Jr, K. Amine, J. Power Sources 2011, 196, 10344.

[40] Z. Zhang, D. Fouchard, J. R. Rea, J. Power Sources 1998, 70, 16.

[41] P. Verma, P. Maire, P. Novák, Electrochim. Acta 2010, 55, 6332.

[42] K. Xu, A. von Cresce, U. Lee, Langmuir 2010, 26, 11538.

[43] A. Ponrouch, E. Marchante, M. Courty, J.-M. Tarascon, M. R. Palacin, Energy Environ. Sci. 2012, 5, 8572.

[44] B. Garcia, S. Lavallée, G. Perron, C. Michot, M. Armand, Electrochim. Acta 2004, 49, 4583.

[45] T. Abe, H. Fukuda, Y. Iriyama, Z. Ogumi, J. Electrochem. Soc. 2004, 151, A1120.

[46] J. Zheng, Y. Hou, Y. Duan, X. Song, Y. Wei, T. Liu, J. Hu, H. Guo, Z. Zhuo, L. Liu, Z. Chang, X. Wang, D. Zherebetskyy, Y. Fang, Y. Lin, K. Xu, L.-W. Wang, Y. Wu, F. Pan, Nano Lett. 2015, 15, 6102.

[47] I. Belharouak, Y.-K. Sun, W. Lu, K. Amine, J. Electrochem. Soc. 2007, 154, A1083.

[48] Y.-Q. Wang, L. Gu, Y.-G. Guo, H. Li, X.-Q. He, S. Tsukimoto, Y. Ikuhara, L.-J. Wan, J. Am. Chem. Soc. 2012, 134, 7874.

[49] J. Wang, J. Polleux, J. Lim, B. Dunn, J. Phys. Chem. C 2007, 111, 14925.

[50] V. Augustyn, J. Come, M. A. Lowe, J. W. Kim, P.-L. Taberna, S. H. Tolbert, H. D. Abruña, P. Simon, B. Dunn, Nat Mater 2013, 12, 518.

[51] M. D. Levi, D. Aurbach, J. Electroanal. Chem 1997, 421, 79.

[52] J. B. Cook, H.-S. Kim, Y. Yan, J. S. Ko, S. Robbennolt, B. Dunn, S. H. Tolbert, Advanced Energy Materials 2016, 6, 1501937.

[53] H.-S. Kim, J. B. Cook, H. Lin, J. S. Ko, S. H. Tolbert, V. Ozolins, B. Dunn, Nat Mater 2017, 16, 454.

[54] J. B. Cook, H.-S. Kim, T. C. Lin, C.-H. Lai, B. Dunn, S. H. Tolbert, Advanced Energy Materials 2017, 7, 1601283.

[55] H.-S. Kim, J. B. Cook, S. H. Tolbert, B. Dunn, J. Electrochem. Soc. 2015, 162, A5083.

[56] G. A. Muller, J. B. Cook, H.-S. Kim, S. H. Tolbert, B. Dunn, Nano Lett. 2015, 15, 1911.

[57] M. J. Frisch, G. W. Trucks, H. B. Schlegel, G. E. Scuseria, M. A. Robb, J. R. Cheeseman, G. Scalmani, V. Barone, B. Mennucci, G. A. Petersson, H. Nakatsuji, M. Caricato, X. Li, H. P. Hratchian, A. F. Izmaylov, J. Bloino, G. Zheng, J. L. Sonnenberg, M. Hada, M. Ehara, K. Toyota, R. Fukuda, J. Hasegawa, M. Ishida, T. Nakajima, Y. Honda, O. Kitao, H. Nakai, T. Vreven, J. A. Montgomery Jr., J. E. Peralta, F. Ogliaro, M. J. Bearpark, J. Heyd, E. N. Brothers, K. N. Kudin, V. N. Staroverov, R. Kobayashi, J. Normand, K. Raghavachari, A. P. Rendell, J. C. Burant, S. S. Iyengar, J. Tomasi, M. Cossi, N. Rega, N. J. Millam, M. Klene, J. E. Knox, J. B. Cross, V. Bakken, C. Adamo, J. Jaramillo, R. Gomperts, R. E. Stratmann, O. Yazyev, A. J. Austin, R. Cammi, C. Pomelli, J. W. Ochterski, R. L. Martin, K. Morokuma, V. G. Zakrzewski, G. A. Voth, P. Salvador, J. J. Dannenberg, S. Dapprich, A. D. Daniels, Ö. Farkas, J. B. Foresman, J. V. Ortiz, J. Cioslowski, D. J. Fox, Gaussian, Inc., Wallingford, CT, USA 2009.

[58] A. D. Becke, J. Chem. Phys. 1993, 98, 5648.

[59] A. McLean, G. Chandler, J. Chem. Phys. 1980, 72, 5639.

요약 (국문 초록)

흑연에서의 용매-리튬 이온 삽입 반응을 이용한 리튬 이온 이차전지 소재 개발

리튬 이온이 흑연으로 삽입되는 반응은 리튬 이온 이차전지에서 중요한 매커니즘이다. 하지만, 리튬 이온과 용매가 흑연으로 함께 삽입되는 반응은 흑연의 층상 구조 박리를 야기한다고 알려져 있기 때문에 이차전지의 수명 특성에 있어 바람직하지 않다고 여겨져 왔다. 본 연구에서는 리튬 이온과 용매가 함께 삽입되는 반응이 반드시 박리를 야기하는 것이 아니라 용매의 종류에 따라 어떤 용매에서는 가역적인 반응이 일어날 수 있음을 증명하였다. 먼저 제 1 원리 계산을 통해 흑연과 리튬 이온-용매 복합체의 화학적 안정성이 가역성에 영향을 끼침을 알아냈고, 실험적으로도 이것을 증명하였다. 또한, 리튬 이온-용매가 함께 삽입되는 반응이 기존의 리튬 이온 삽입 반응보다 훨씬 더 높은 출력 특성을 보이는 것을 증명하였다. 이러한 높은 출력 특성은 리튬 금속이 석출되는 것을 방지하여

이차전지가 안전하게 작동하도록 돕는다. 보다 구체적으로, 리튬 이온–용매가 함께 삽입되는 반응은 1 A g^{-1} 정도의 고전류에서도 이론 용량의 87%의 용량을 내는 것을 확인하였다. 이러한 높은 출력 특성의 원인은 첫째, 리튬 이온–용매 복합체에서 마지막 탈용매화 과정이 없는 것, 둘째, 흑연과 전해질 사이 계면에서 박막이 적게 형성되는 것, 그리고 셋째, 전기 용량적인 특성을 띠는 전하 이동 반응에 기인한 것으로 생각된다. 본 연구는 이차전지 기술에 있어서 빠르고 가역적인 리튬 이온–용매 복합체 삽입 반응의 활용을 향한 첫 단계가 될 것이다.

주요어: 흑연, 리튬 이온 이차전지, 삽입 반응, 고출력 이차전지, 제1원리 계산